Tropical low formation and intensification over land as seen in ECMWF analyses.

Gerard Kilroy[a], Roger K. Smith[a]*, M. T. Montgomery[b]
[a] *Meteorological Institute, Ludwig-Maximilians University of Munich, Munich, Germany*
[b] *Dept. of Meteorology, Naval Postgraduate School, Monterey, CA*
*Correspondence to: Dr. Gerard Kilroy, Meteorological Institute, Ludwig-Maximilians University of Munich, Theresienstr. 37, 80333 Munich, Germany. E-mail: gerard.kilroy@lmu.de

Case studies of the formation and intensification over land of three tropical lows in northern Australia are presented based on European Centre for Medium Range Weather Forecast (ECMWF) analyses. The aim is to investigate the generality of recent results concerning the dynamics and thermodynamics of tropical lows. Consistent with these results, the findings indicate that the essential processes of formation and intensification are the same over land as those that operate over the ocean. An important element of the intensification process is the requirement that bursts of deep convection are able to persist near the circulation centre, which, in turn, requires the maintenance of convective instability through surface moisture fluxes. The convectively-induced import of air from the moist monsoonal environment provides an effective shield against the adverse effects of dry air intrusion from the Australian continent.

Key Words: Tropical depressions; tropical lows, tropical cyclogenesis, monsoonal lows

Received May 11, 2016; Revised ; Accepted

Citation: . . .

1. Introduction

During the Australian 'Wet Season' (November-April), a trough of low pressure lies south of the equator at Australian longitudes. Early in the wet season, this so-called monsoon trough forms to the north of the Australian continent. Later the trough moves southwards and at times may lie over the continent. At such times it is common for tropical lows to develop over land somewhere along the trough. Occasionally a low may form close enough to the coast to be a particular concern to forecasters, since if the low moves over the sea, it has a strong chance of developing into a tropical cyclone. Even if the low remains over land, or if it forms over the sea and moves over the land (sometimes as a land-falling tropical cyclone), it can produce prodigious amounts of rain and can cause serious flooding over a significant area. An important landmark study of tropical cyclogenesis during the Australian monsoon is that of McBride and Keenan (1982).

Like tropical cyclones themselves, the lows that form over land do so in a region with relatively sparse conventional data coverage and until recently, little was known in detail about their formation pathways and structure. In particular, a conceptual model that might be of use to operational forecasters was, to our knowledge, unavailable. One of the most important questions from a forecasting perspective is whether or not a low will develop in the forecast area and when? While answering the last question would inevitably require the use of guidance from numerical forecast systems, an improved understanding of the basic mechanisms would be helpful.

Advances in understanding maritime tropical cyclogenesis have emerged from seminal studies by Hendricks *et al.* (2004) and Montgomery *et al.* (2006), which pointed to the important role of rotating deep convection, and that of Dunkerton *et al.* (2009), who examined the nurturing role of a tropical wave and presented a new framework for describing how such hybrid wave-vortex structures develop into tropical depressions. These and related work by Tory *et al.* (2006a,b, 2007) vis-à-vis tropical cyclogenesis in the Australian region are summarized by Smith *et al.* (2015), together with two earlier studies relevant to this region by Foster and Lyons (1984) and Davidson and Holland (1987).

The Tory *et al.* studies raise the question as to whether the development of monsoon depressions over land is fundamentally different from the genesis of tropical cyclones over the sea.

In a first attempt to address this question, Smith *et al.* (2015) carried out an analysis of tropical low formation in the Australian monsoon during January 2013 based on ECMWF analyses. The focus was on three lows that developed on the monsoon shear line, two of which eventually became tropical cyclones. Smith *et al.* gave interpretations of the formation of these disturbances in terms of vorticity dynamics. An important feature of the two lows that eventually became tropical cyclones was found to be the occurrence of persistent bursts of (parameterized) deep convection near the circulation centre.

Kilroy *et al.* (2016) carried out a case study of a tropical low that formed near Darwin, Australia in January 2014, again on the basis of ECMWF analyses. This low continued to intensify as it moved southwards over land. A moisture budget showed that the horizontal transport of moisture into a column (more specifically, square columns of 2^olon $\times 2^o$lat, 4^olon $\times 4^o$lat and 6^olon $\times 6^o$lat, centred on the minimum geopotential at 850 mb) of atmosphere centred on the low was approximately equal to the moisture lost by precipitation, and that the contribution to the moisture budget by surface fluxes was comparatively small. Nevertheless, despite their small contribution to the moisture budget, the surface fluxes are necessary to maintain conditionally unstable conditions near the vortex centre so that deep convective bursts can continue to occur. Similar results were found in a convection-permitting numerical study of a different monsoonal low that developed over land by Tang *et al.* (2016).

Consistent with the analyses of Smith *et al.* (2015), those by Kilroy *et al.* (2016) and Tang *et al.* (2015) indicated that the intensification of a tropical low requires the occurrence of repeated bursts of deep convection occurring near the circulation centre. From a vorticity perspective, the convectively-induced lower-tropospheric convergence promotes the further concentration of cyclonic vorticity near the circulation centre and thereby an enhancement of the local circulation about the centre. The increase in circulation amounts to an increase in the local tangential wind speed and, through approximate gradient wind balance above the boundary layer, to a lowering of the central pressure. This feature was highlighted in a series of convection-permitting sensitivity experiments by Tang *et al.* (2016), who found that bursts of deep convection near the circulation centre were accompanied invariably by pulses of intensification.

1.1. *The present study*

As a further step to developing a basic conceptual model of tropical lows over and to examine the generality of recent findings discussed above, we have undertaken case studies of three further events, all of which intensified while over land and provided a challenge to local forecasters. The case studies are based on selected kinematic, dynamic and thermodynamical fields extracted from ECMWF analyses.

The paper is organized as follows. In section 2 we summarize the data used for the study and introduce the three cases to be analysed. The three subsequent sections present the analyses of each case. There follows a section synthesizing the findings from these events and finally a section detailing the conclusions.

2. Data, cases and methodology

The ECMWF analyses used for this study are from a global 4DVAR analysis and prediction system (see e.g. Bauer *et al.* 2011). Forecasts from this system are considered by forecasters to be as good as any available. The analyses are available at the surface and at 21 or 25 pressure levels between 1000 mb and 1 mb (the number of pressure levels was increased from 21 to 25 on 6 November 2007). The data cover the domain from 100^{o}E to 160^{o}E and from the Equator to 30^{o}S, with a horizontal grid spacing of 0.125 deg. The case studies are based on selected kinematic, dynamic and thermodynamical fields extracted from these analyses.

Three cases are chosen here for investigation: the unnamed tropical low that formed near Darwin in January 2006 during the Tropical Warm Pool International Cloud Experiment (TWP-ICE) - see May *et al.* (2008a,b); the low that became Tropical Cyclone Georges in February 2007; and the low that became Severe Tropical Cyclone Carlos in February 2011. Interest is confined to the early stages of formation while the systems are centred over land. A numerical simulation study of the 2006 unnamed low is discussed in a recent paper by Tang *et al.* (2016).

As in Smith *et al.* (2015) and Kilroy *et al.* (2016), interpretations of formation are given in terms of vorticity dynamics. Vertical vorticity is useful in characterizing local rotation, but it may be associated also with regions of horizontal shear deformation. These deformation regions are detrimental to the formation of concentrated vortices. Regions where the vorticity is rotation dominated, as opposed to strain dominated, are regions that are favourable for vortex development. For this reason, we analyse the Okubo-Weiss (OW) parameter (Dunkerton *et al.* (2009)) to highlight regions where the flow is rotationally dominant. Rotationally dominant regions are regions where patches of enhanced vertical vorticity are most capable of congealing to form a monopole structure.

3. The unnamed low of January 2006

This tropical low formed off the north coast of the Top End around 00 UTC 22 January. Figure 1 shows the subsequent track together with the intensity and magnitude of the mean vertical wind shear. The vertical shear is characterized here by the magnitude of the vector velocity difference between 850 mb and 200 mb averaged over mesoscale columns 2^olon$\times 2^o$lat, 4^olon$\times 4^o$lat, and 6^olon$\times 6^o$lat centred on the location of the minimum geopotential at 850 mb[1]. The intensity is characterized by the maximum wind speed at 850 mb within the 2^olon $\times 2^o$lat column.

During the first few days shown, the low moved northwards, and then westwards, and strengthened in an environment of moderate (≈ 10 m s^{-1}) vertical shear, making landfall in the Darwin area around 18 UTC 24

[1]We compute first the local vector velocity difference and then compute the average over the column. Because of the linearity of the shear vector calculation, the method is equivalent to computing the vector shear from the difference in the areal average velocity at the two levels. This is equivalent to the method adopted by DeMaria and Kaplan (1994, p213) as a basis for their Statistical Hurricane Intensity Prediction Scheme (SHIPS).

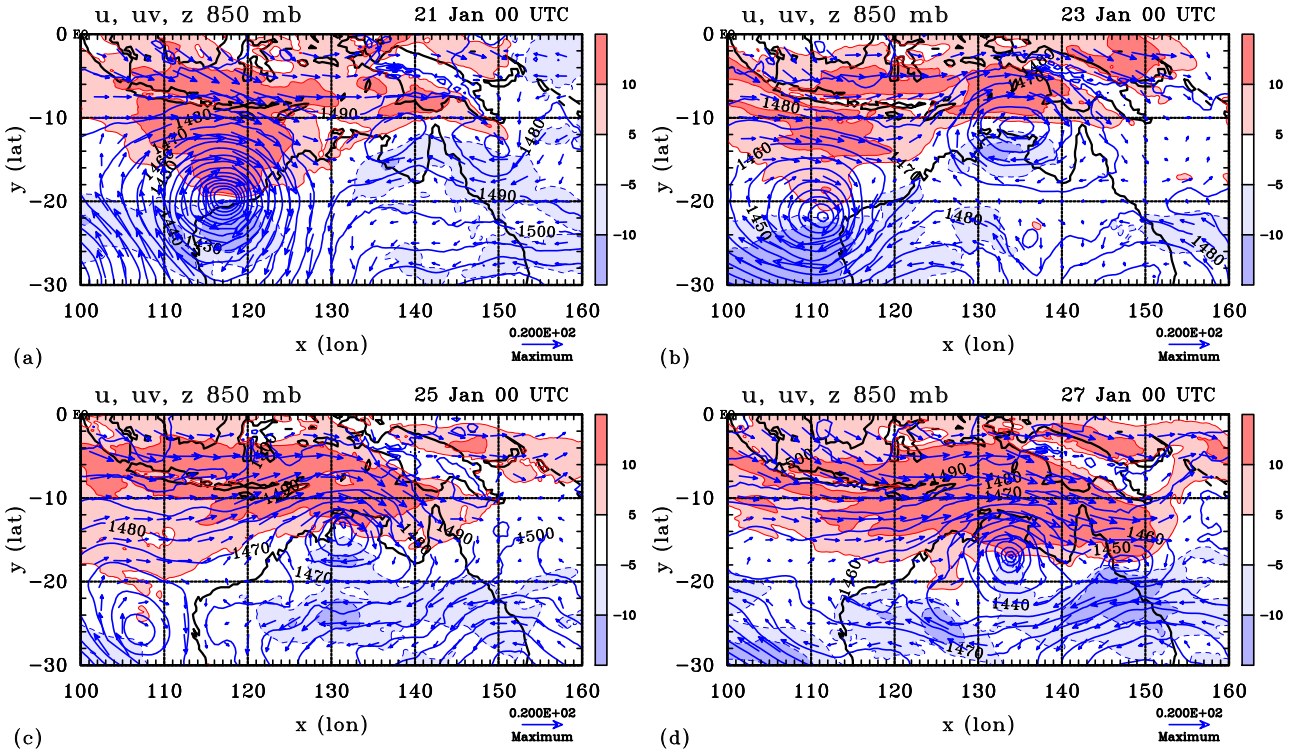

Figure 2. Wind vectors at 850 mb together with contours of the zonal wind component and geopotential height at 0/0 UTC on (a) 21 January, (b) 23 January, (c) 25 January and (d) 27 January 2006 illustrating the formation of the Northern Territory low. Westerly wind component greater than 5 m s^{-1} shaded pink, that greater than 10 m s^{-1} shaded red. Easterly winds greater than 5 m s^{-1} in magnitude shaded light blue, those greater than 10 m s^{-1} in magnitude shaded blue. Contour interval for geopotential height 10 m. Solid contours positive, dashed contours negative. Wind vectors should be compared to the reference vector (20 m s^{-1}) at the bottom right of each panel.

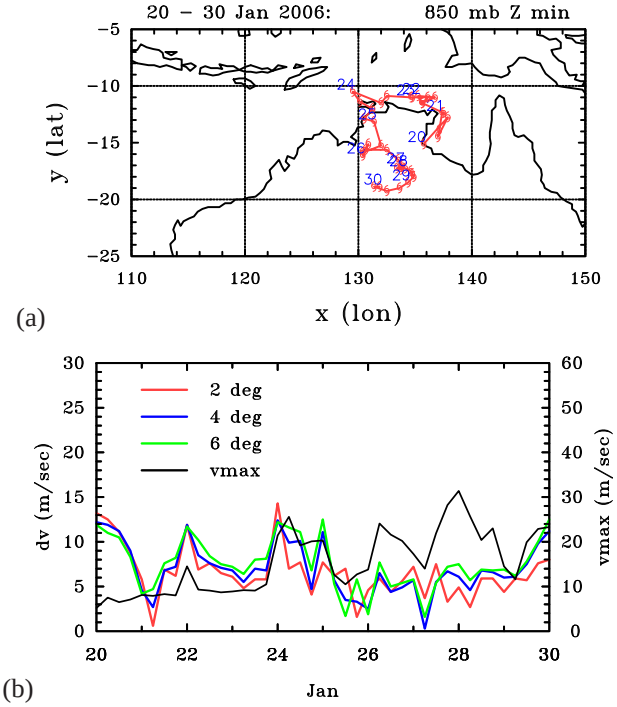

Figure 1. (a) Track of the NT tropical depression: 20-30 January 2006. Positions of the minimum geopotential at 850 mb indicated by cyclone symbols every 6 h. Positions at 00 UTC shown by date. (b) Mean vertical wind shear, characterized by the magnitude of the vector velocity difference between 850 mb and 200 mb, averaged over mesoscale columns 2^olon $\times 2^o$lat, 4^olon $\times 4^o$lat, and 6^olon $\times 6^o$lat centred on the location of the minimum geopotential at 850 mb and maximum wind speed (vmax) at 850 mb within the 2^olon $\times 2^o$lat column.

January. Thereafter it drifted southwards down the western border of the Northern Territory and weakened. Coincident with a weakening of the shear from 12 UTC on 25 January, the low re-intensified and around 00 UTC 26 January it began to track southeastwards, achieving its maximum intensity of about 30 m s^{-1} at 18 UTC 27 January. Thereafter, it gradually weakened and from 00 UTC 29 January began to move slowly southwestwards. The low initiated an active monsoon onset over the northern Top End, and brought heavy rainfall to many parts of the western Northern Territory.

Figure 2 shows the wind structure at 850 mb together with the wind vectors and the contours of zonal wind component and geopotential height at 00 UTC on 21, 23, 25 and 27 January 2006. On 21 January, the wind field is dominated by Tropical Cyclone Daryl located near 117^oE, 20^oS at this time. There is a weak geopotential low located over the Gulf of Carpentaria, although at this time there is no noticeable circulation associated with the low. By 00 UTC 23 January (panel (b)), the large scale flow has changed dramatically with a strengthening of the westerlies north of Darwin, the development of a broad circulation over the Top End, and a lowering of the 850 mb geopotential heights near the centre of this circulation. At this time the low centre is located just north of the coastline. By 00 UTC 25 January (panel c), the geopotential low is centred over land, essentially above Darwin, but has not deepened, although the region of strong westerlies has increased in areal extent. In the following 48 h the system moves southwards over land, intensifying as it does so (panel d). From 25 January onwards, the magnitude of the vertical shear decreases and, despite being located over land, the low continues to strengthen. A key feature to note is that the easterlies to

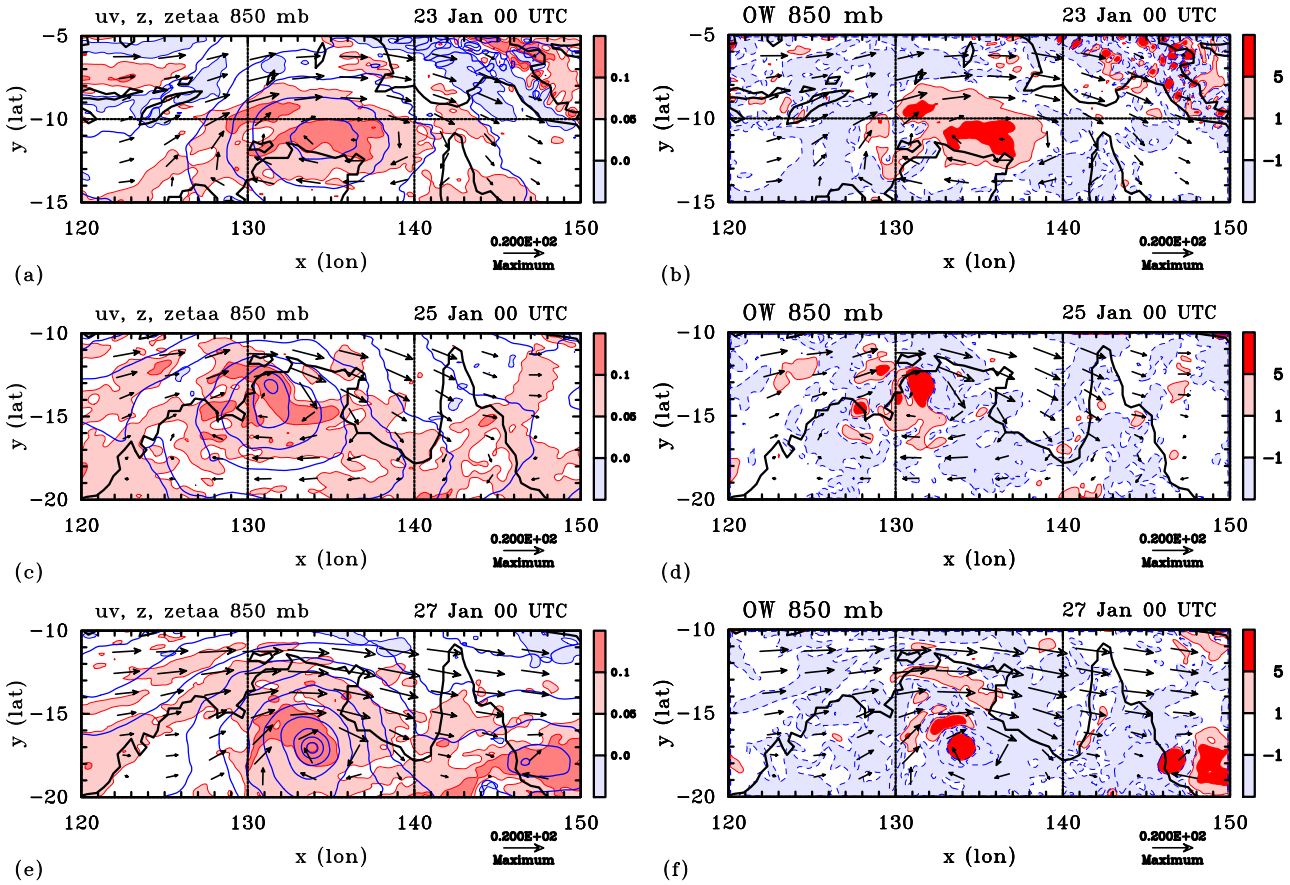

Figure 3. Left panels: wind vectors at 850 mb together with contours of the absolute vorticity (shaded) and geopotential height (thick blue contours) at 00 UTC on (a) 23 January, (c) 25 January and (e) 27 January 2006 illustrating the formation of the low. Contour interval for geopotential height is 10 m. Absolute vorticity shading as shown on the label bar multiplied by 10^{-3} s^{-1}. Cyclonic values of vorticity are positive (red/pink shading), anticyclonic values are negative (light blue shading). Right panels: contours of the Okubo-Weiss (OW) parameter (shaded) at 00 UTC on (b) 23 January, (d) 25 January, and (f) 27 January 2007 illustrating environment during the formation of the low. Contour interval for geopotential height is 10 m. OW shading as shown on the label bar multiplied by 10^{-8} s^{-2}. Positive values have pink/red shading; negative values light blue shading. Solid contours positive, dashed contours negative. Wind vectors should be compared to the reference vector (20 m s^{-1}) at the bottom right of each panel.

the south of the system remain mostly weak throughout the period shown in Fig. 2, in contrast to systems described in Smith *et al.* (2015) and Kilroy *et al.* (2016).

A vorticity and OW perspective of the foregoing development is illustrated in Fig. 3. This shows the vertical component of absolute vorticity, the corresponding wind vectors, the contours of geopotential height at 850 mb, and the distribution of the OW parameter at the 850 mb level at 00 UTC on 23 January, 25 January and 27 January. At 00 UTC 23 January, the most prominent feature in the absolute vorticity field is the broad region of elevated cyclonic values[2] north of the Top End. There is a coherent region of positive OW values within the weak vortex circulation centred over the elevated vorticity values. This OW-feature is coherent up to 500 mb (not shown) and is one factor indicating that the vortex has potential for further development. At 00 UTC 25 January, the areal extent of both the positive vertical vorticity and OW regions has decreased. By 00 UTC 27 January, the system has intensified further, although the size of the enhanced positive regions of vertical vorticity and OW remain relatively small when compared to the events discussed in Smith *et al.* (2015) and Kilroy *et al.* (2016). A reduction in the areal extent of the positive OW region would be detrimental to deep convection around the periphery of the vortex, reducing the ability of such clouds to induce inflow and converge vorticity.

As a step towards understanding the role of deep convection in the spin up of low-level vorticity, we examine next areas of strong vertical velocity at 500 mb, a proxy for regions of deep convection in the analyses, as the vortex evolves. Here strong refers to a vertical p-velocity $\omega < -2.0$ Pa s^{-1}. The distribution of vertical motion is shown in Fig. 4 at 00 UTC on 24 and 25 January with the horizontal wind fields at 850 mb superimposed. On 24 January, strong vertical motion (indicated by the yellow contours in Fig. 4a) occurs near the centre of the circulation. Following this "pulse" of deep convection, the low has a larger maximum wind speed (Fig. 1b). On 25 January at 00 UTC there is a region of marked subsidence near the vortex centre, and there is a subsequent reduction in the maximum wind speed at this time (Fig. 1b).

Figure 5 shows time-height cross sections of various quantities averaged over a square column of 2^olon $\times 2^o$lat centred on the minimum geopotential at 850 mb. These quantities include the vertical mass flux (approximated here by $-\omega/g$), the temperature deviation from the box averaged temperature at the start of the time series, the relative humidity, and the pseudo-equivalent potential temperature, θ_e. Shown also is a time-height cross section of the circulation around the column and a simple moisture budget

[2]For plotting, the sign of the vertical vorticity is reversed so that cyclonic vorticity is positive.

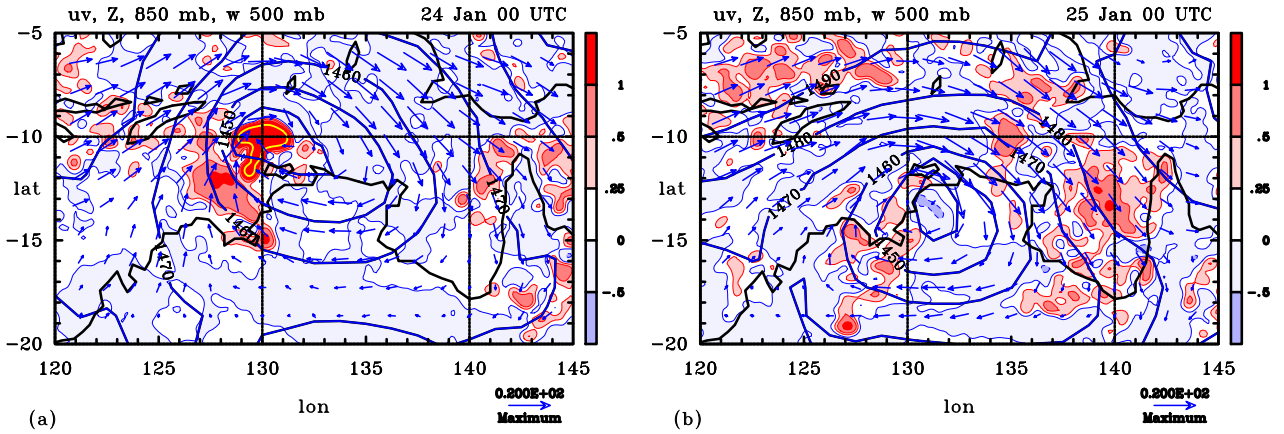

Figure 4. Wind vectors, contours of geopotential height together with contours of the vertical velocity at 500 mb at 00 UTC on 24 and 25 January 2006, illustrating the formation. Contour interval for geopotential height is 10 m. Vertical p-velocity (ω) shading as shown on the label bar in units Pa s^{-1}. Upward vertical velocities (negative values of ω) are plotted as positive (red/pink shading); negative values of vertical velocity (positive values of ω) are plotted negative (light blue/blue shading). Strong regions of upflow are highlighted by the yellow contour (-2 Pa s^{-1}). Solid contours positive, dashed contours negative. Wind vectors should be compared to the reference vector (20 m s^{-1}) at the bottom right of each panel.

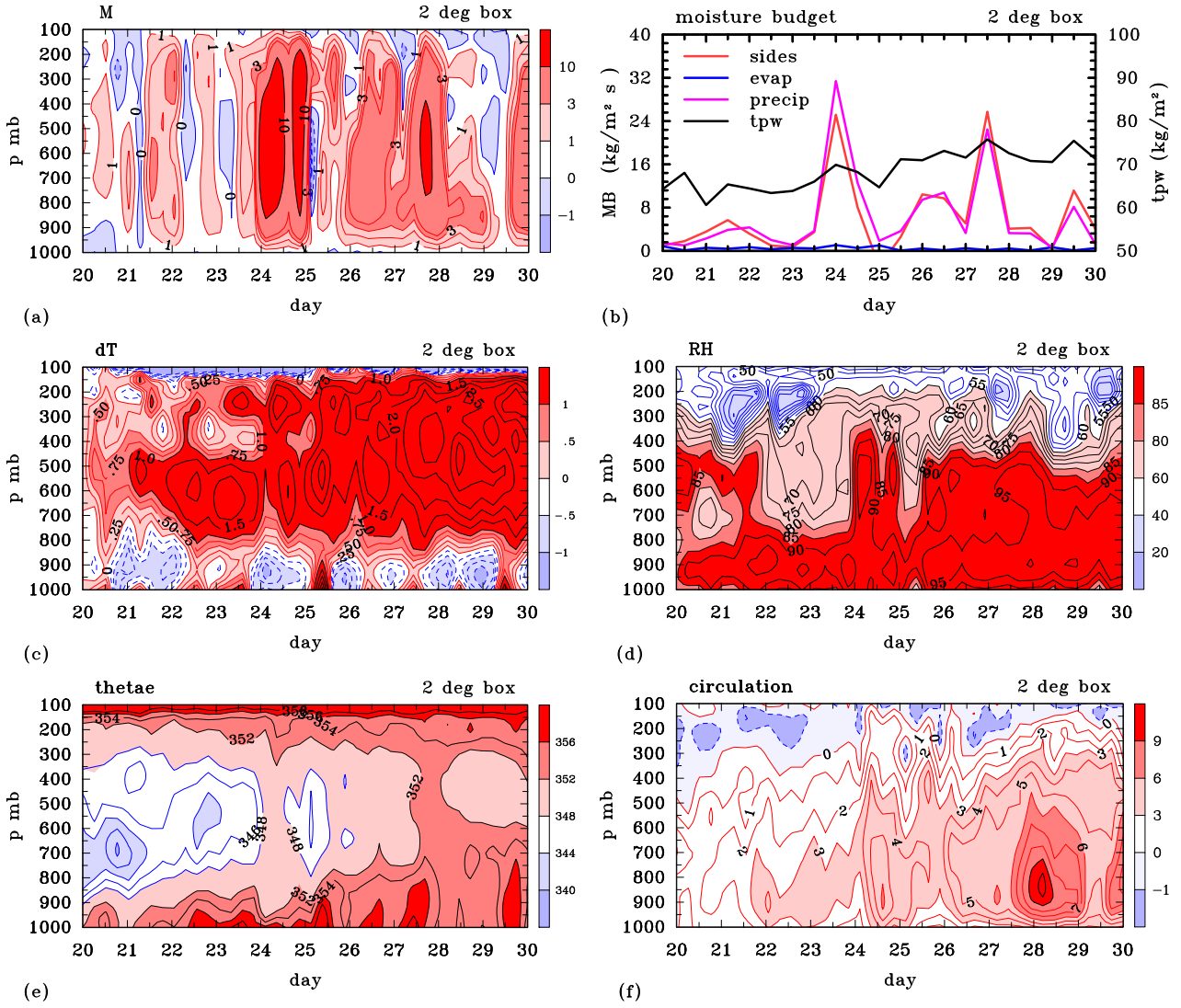

Figure 5. Time-height cross-section of system averaged quantities within a column 2^olon $\times 2^o$lat, centred on the location of the minimum geopotential at 850 mb for the development of the unnamed low of January 2006. These include (a) the vertical mass flux per unit area (units kg s^{-1} m^{-2}) (c) the temperature deviation from that at the start of the time series, (d) the relative humidity (in per cent), and (e) pseudo-equivalent potential temperature (in K). Panel (f) shows the normalized circulation around the column (units m s^{-1}). Panel (b) shows the sources and sinks of moisture including the contributions by surface evaporation, precipitation and the horizontal transport of moisture averaged over a 2^olon $\times 2^o$lat column centred on the location of the minimum geopotential at 850 mb. The horizontal transport of moisture is calculated by summing the vertically integrated fluxes of moisture into the column and then dividing the sum by the area of the column so that all terms have the units kg m $^{-2}$ s $^{-1}$. The values shown here have been multiplied by 10^5. Shown also is the total precipitable water in kg m $^{-2}$.

(details on how this budget is calculated are given in Kilroy *et al.* 2016).

Notable features in the vertical mass flux field are the two "bursts" of deep convection that occur on 24 January (Fig. 5a) and another one seen around 18 UTC on 27 January. The first two bursts are accompanied by a decrease in the magnitude of vertical shear within the column and to an increase in the maximum tangential wind speed (see Fig. 1b). Not surprisingly, these bursts are accompanied by sharp peaks in the precipitation and a marked increase in the moisture flux into the column associated with the low-level convergence induced by the convection (Fig. 5b).

As in the tropical low examined by Kilroy *et al.* (2016), the total moisture supply to the system is dominated by the convectively-induced import of moisture into the sides of the column, while the contribution from surface moisture fluxes is comparatively small[3]. The import of air from the moist monsoonal environment provides an shield against the adverse effects of dry air intrusion from the Australian continent. Of course, as noted by Kilroy *et al.* (2016) and Tang *et al.* (2016), the availability of substantial column moisture, by itself, does not mean that deep convection will occur or be sustained. Deep convection requires the presence of conditional instability and sustained deep convection requires that this instability be maintained. Thus, while surface moisture fluxes are a small component of the overall moisture budget, they are important for vortex intensification in maintaining conditional instability in the central region of the vortex. Evidence for this maintenance is provided by periodic increases in low level θ_e discussed below.

In terms of surface latent heat flux, the daytime values at 00 UTC on 22, 23, 24, 25, 26, 27, 28 January averaged over the 2^olon$\times 2^o$lat square column are 157, 123, 245, 231, 103, 114 and 99 W m^{-2}, respectively, and at 12 UTC on these days are 71, 101, 118, 17, 28, 32, and 23 W m^{-2}, respectively. Unfortunately, the fluxes are available only 12 h intervals so that it is not possible to determine a reliable 24 h mean.

Following the convective bursts on 24 January, there are several periods when the precipitation inside the column is nearly zero. At 00 UTC 25 January, the lateral moisture flux into the column is negative (Fig. 5b), a feature that is presumably associated with subsidence within the column, and the TPW is lower than earlier. The brief period of marked subsidence on 25 January 00 UTC (Fig. 5a) is accompanied by a decrease in both the mid-level relative humidity and θ_e, but the system slowly recovers with a progressive elevation of mid-level θ_e over the ten day period shown. There are periodic increases in low level θ_e as well. These are likely to be associated with surface moisture fluxes and indicate maintenance of convective instability in the column. During this same period, there is a general warming of the middle and upper troposphere, but cooling in the lower troposphere, mostly below 900 mb and greater than 1^oC in magnitude. The warming is presumably associated with latent heat release in convection and the cooling with convectively-induced mesoscale downdraughts.

The circulation around the column remains relatively weak until the second convective burst at 18 UTC 27 January (Fig. 5f). At this time, the system is far inland (Fig. 1a). Perhaps significantly, the largest circulation at any one time is found in the lower troposphere, typically at pressures above 800 mb (i.e. altitudes below 2 km).

In summary, the unnamed low of January 2006 developed slowly at first while immersed in an environment of moderate vertical shear, until a day of sustained convective bursts occurred close to the circulation centre. At that point the mean vertical shear reduced and the low intensified while over land. As noted by Kilroy *et al.* (2016), it is not possible to conclude from the analyses that the decrease in vertical shear led to the intensification or whether the intensification, itself, led to the reduction in shear.

4. Formation of Tropical Cyclone George (2007)

Severe Tropical Cyclone George was the most destructive cyclone to affect Western Australia since Tropical Cyclone Joan in 1975. Figure 6a shows the track of the cyclone and its precursor low during the period of interest: 27 February to 9 March. The cyclone was named on 3 March while over the Joseph Bonaparte Gulf and it became a Severe Tropical Cyclone (Category 3) on the evening of 7 March. Interest is focused here on the formation of its precursor disturbance over the Top End of Australia.

As in Fig. 1b, Fig. 6b shows the maximum wind speed at 850 mb within the 2^olon $\times 2^o$lat column centred on the minimum geopotential at 850 mb is shown together with the magnitude of the mean vertical wind shear between 850 mb and 200 mb over various mesoscale columns. From early on, even in the presence of moderate to strong vertical wind shear ($\approx 10-15$ m s^{-1}), the precursor to George has a relatively large maximum wind speed (about 25 m s^{-1}). This maximum is more a reflection of the relatively strong environmental westerlies than the strength of the disturbance, itself. On 00 UTC 3 March the vertical wind shear decreases sharply in magnitude (to less than 5 m s^{-1}) and the system intensifies over water to a cyclone.

Figure 7 shows the wind vectors at 850 mb together with the contours of the zonal wind component and geopotential height at 00 UTC on 27, 28 February and 2, 4 March 2007. On 27 February, the wind field is dominated by strong westerlies north of 10^oS, and strong widespread easterlies over much of continental Australia. There are two low pressure systems present at this time, one located over the Top End of the Northern Territory, and the other located over the ocean north-east of Australia. We focus our interest on the system located over the Top End, which develops into Tropical Cyclone George. At this time there is no noticeable circulation associated with the low, although the maximum wind speed is relatively large (Fig. 6), a reflection of the strong monsoonal flow.

On 28 February the low has deepened considerably and there is a noticeable circulation associated with it. Two days later, on 2 March, the broad-scale flow is much the same, although the easterlies over the continent have weakened. On 4 March there are significant differences from 48 hours earlier, with the easterlies having increased in strength over much of the continent, but the low has only slightly deepened (the 850 mb geopotential minimum decreases by 23 m). Beyond 00 UTC 4 March, the low intensifies significantly with the maximum wind speed reaching over 50 m s^{-1} on 7 March.

A vorticity and OW perspective of the foregoing development is illustrated in Fig. 8. On 27 February the

[3]A discussion of how the moisture budget is calculated and some issues about closure are found in Kilroy *et al.* (2016, section 5.3 and footnote 10).

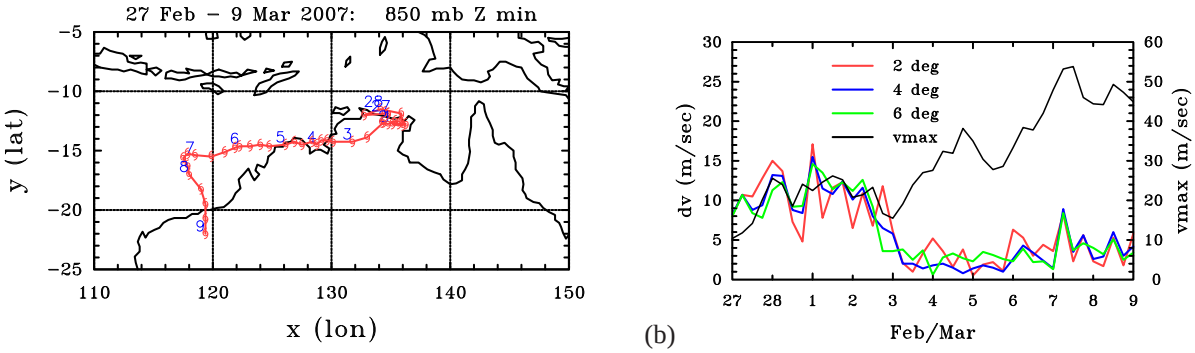

Figure 6. (a) Track of the tropical depression that developed into Tropical Cyclone George (2007). Positions of the minimum geopotential at 850 mb indicated by cyclone symbols every 6 h. Positions at 00 UTC shown by date. (b) Mean vertical wind shear, characterized by the magnitude of the vector velocity difference between 850 mb and 200 mb, averaged over mesoscale columns 2^olon $\times 2^o$lat, 4^olon $\times 4^o$lat, and 6^olon $\times 6^o$lat centred on the location of the minimum geopotential at 850 mb and maximum wind speed at 850 mb within the 2^olon $\times 2^o$lat column.

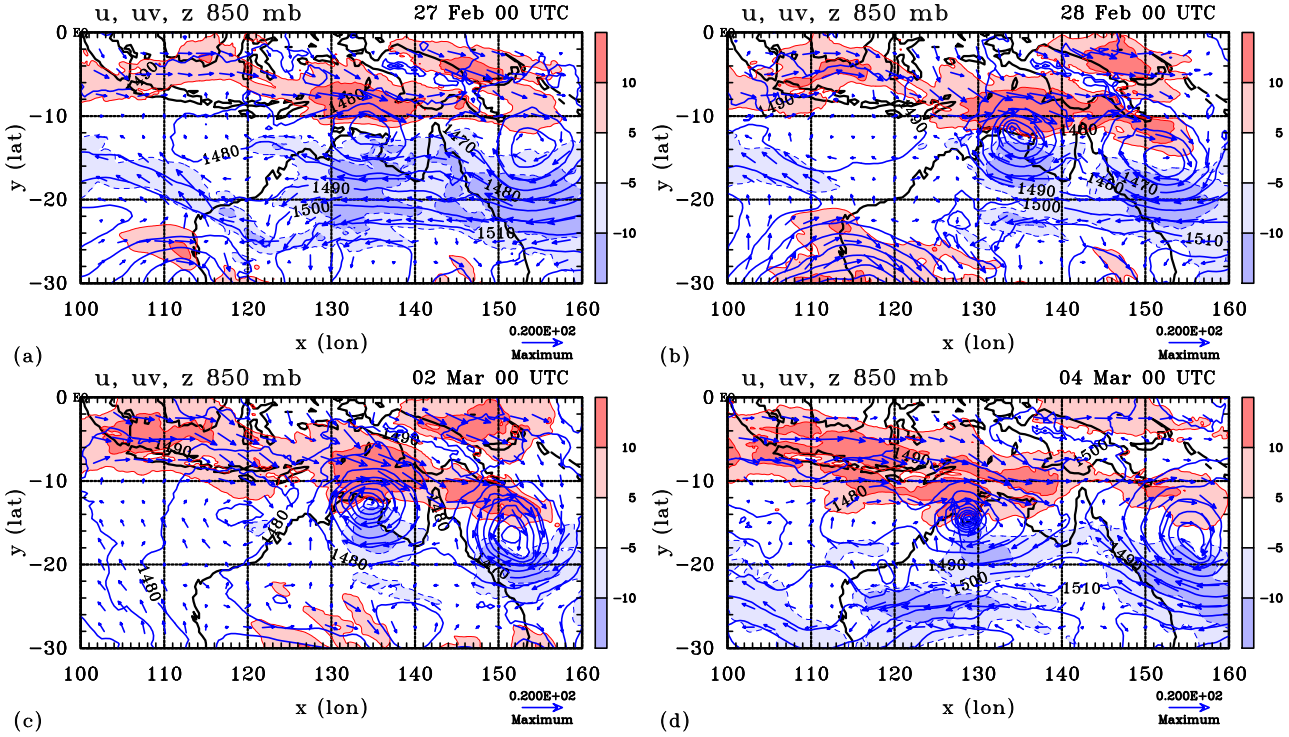

Figure 7. Wind vectors at 850 mb together with contours of the zonal wind component and geopotential height at 00 UTC on (a) 27 February, (b) 28 February, (c) 02 and (d) 04 March 2007 illustrating the formation of the low. Westerly wind component greater than 5 m s^{-1} shaded pink, that greater than 10 m s^{-1} shaded red. Easterly winds greater than 5 m s^{-1} in magnitude shaded light blue, those greater than 10 m s^{-1} in magnitude shaded blue. Contour interval for geopotential height is 10 m. Solid contours positive, dashed contours negative. Wind vectors should be compared to the reference vector (20 m s^{-1}) at the bottom right of each panel.

most prominent feature in the absolute vorticity is the broad region of elevated positive values around the Top End, with elevated positive regions also to the east and west. There is a coherent region of strong positive OW values near the circulation centre. Animations of the fields for the next 48 h indicate that the patches of elevated vertical vorticity surrounding the system are rolled up into the low centre (not shown). The region of strong positive OW persists until 1 March and is somewhat larger in size than that in the January 2006 case (compare right panels of Figs. 3 and 8).

We examine next areas of strong vertical p-velocity at 500 mb as defined earlier. These areas are shown in Fig. 9 with the wind fields at 850 mb superimposed at 00 UTC on 27 February, 1, 3 and 4 March 2007. On 27 February there are patches of deep convection surrounding the geopotential low, although values exceeding $\omega < -2.0$ Pa s^{-1} are not present at this stage. On 1 and 3 March there are regions of strong deep convection (characterized by yellow contours) within the vortex circulation, although not within a 2^olon $\times 2^o$lat column centred on the geopotential low. On 4 March the strong updraughts are located close to the circulation centre. Over the next few days strong convective bursts continue to occur near the circulation centre and the low intensifies (see below).

Figure 10 shows time-height cross sections of various quantities averaged over a square column of 2^olon $\times 2^o$lat centred on the minimum geopotential at 850 mb. These quantities are the same as those shown previously for the 2006 unnamed low in Fig. 5. Notable features in the vertical mass flux field are the "bursts" of strong convection occurring sporadically until 4 March, and then regularly afterwards.

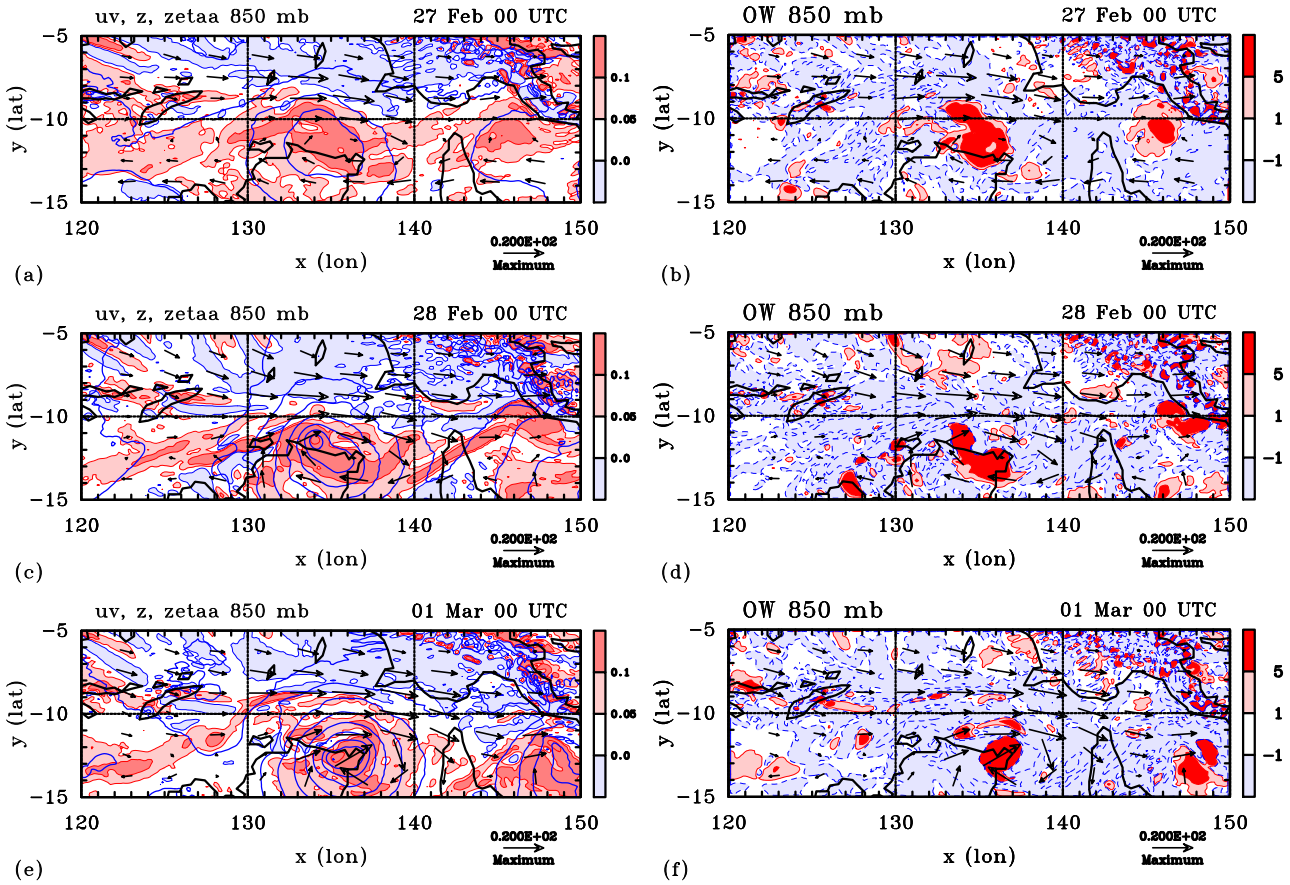

Figure 8. Left panels: wind vectors at 850 mb together with contours of the absolute vorticity (shaded) and geopotential height (thick blue contours) at 00 UTC on (a) 27 February, (c) 28 February and (e) 1 March 2007 illustrating the formation of the low. Contour interval for geopotential height is 10 m. Absolute vorticity shading as shown on the label bar multiplied by 10^{-3} s^{-1}. Cyclonic values of vorticity are positive (red/pink shading), anticyclonic values are negative (light blue shading). Right panels: contours of the Okubo-Weiss (OW) parameter (shaded) at 00 UTC on on (b) 27 February, (d) 28 February and (f) 1 March 2007 illustrating environment during the formation of the low. Contour interval for geopotential height is 10 m. OW shading as shown on the label bar multiplied by 10^{-8} s^{-2}. Positive values have pink/red shading; negative values light blue shading. Solid contours positive, dashed contours negative. Wind vectors should be compared to the reference vector (20 m s^{-1}) at the bottom right of each panel.

In terms of a moisture budget, the burst on 1 March is associated with a local maximum in precipitation, although there is little precipitation within the 2^olon $\times 2^o$lat column over the next two days. These minima in precipitation are not found in the 4^olon $\times 4^o$lat column (not shown), suggesting that deep convection was still occurring on these days, but outside the 2^olon$\times 2^o$lat column. From 4 March onwards, bursts of deep convection, characterized by pulses of enhanced vertical mass flux, occur within the 2^olon$\times 2^o$lat column. These bursts are accompanied by an increase in the flux of moisture converging into the column and also by an increase of precipitation falling out of the column.

The contribution of surface moisture fluxes increases progressively with time, reaching a maximum on 7 March 12 UTC, when the system lay over the sea for the second time, north of Western Australia (Figure 6). In terms of surface latent heat flux, the mean values at 00 UTC on 3, 4, 6 and 12 UTC 7 March are 126, 264, 459, 715 W m^{-2}, respectively. Thus, typical flux values over the sea over the 2^olon$\times 2^o$lat square column are 2-5 times larger when the system is over the sea. Moreover, there is a substantial diurnal variation of the surface latent heat flux over land with daytime values being up to four times larger than night time values.

Note that, from a moisture budget perspective, the moisture supply into the system is dominated by the transport of moisture into the sides of the column, even when the 2^olon$\times 2^o$lat square column lies entirely over the sea (from 12 UTC 5 March until 12 UTC 8 March) over the sea.

As in the case of the unnamed low, there is a general warming of the middle and upper troposphere (Figure 10(c)), but some cooling in the lower troposphere until 6 January when the system is well out over the sea (Figure 6(a)). In George, the relative humidity is generally high throughout the lower half of troposphere, with values mostly exceeding 85% (Figure 10(d)). Values of mid-level θ_e are generally larger than for the unnamed low (compare Figure 10(e) with Figure 10(e)), but there is still some elevation of θ_e at low levels except at 00 UTC on 3 February when the system is furthest from the coast (Figure 6(a)). At this time, there is major cooling Figure 10(c)) and the mass flux signature is weak at low levels (Figure 10(a)) suggesting a lull in active deep convection. Up to this time there are again periodic increases in low level θ_e, indicate maintenance of convective instability by surface fluxes.

The circulation around the 2^olon $\times 2^o$lat column shows a marked increase following the convective burst on 1 March, but weakens again the next two days in the absence of strong deep convection within the column. Once continuous bursts of strong deep convection flare up within the column on 4 March, the circulation strengthens markedly and grows in depth. The temperature difference fields averaged over

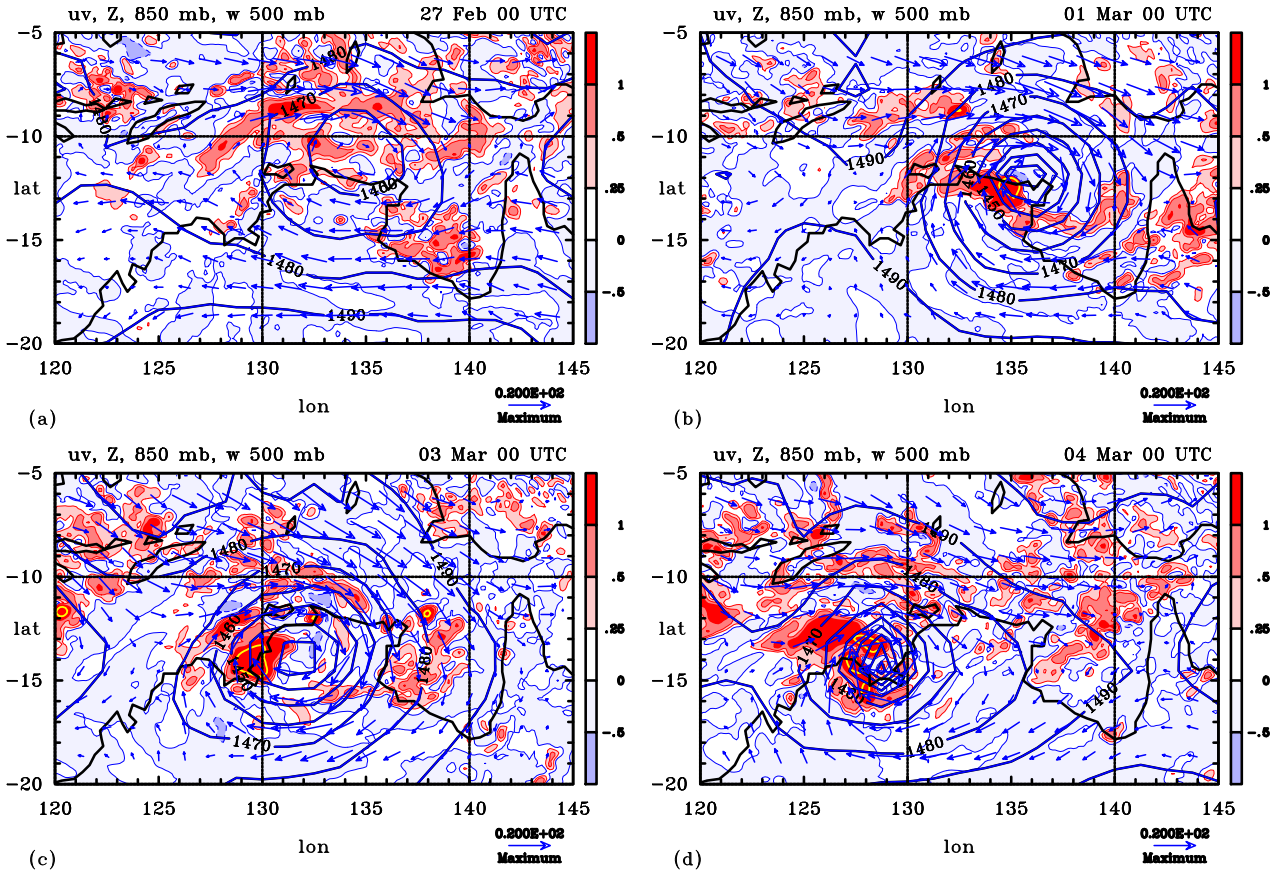

Figure 9. Wind vectors, contours of geopotential height together with contours of the vertical velocity at 500 mb at 00 UTC on several days in February and March 2007, illustrating the formation. Contour interval for geopotential height is 10 m. Vertical p-velocity (ω) shading as shown on the label bar in units Pa s^{-1}. Upward vertical velocities (negative values of ω) are plotted as positive (red/pink shading); negative values of vertical velocity (positive values of ω) are plotted negative (light blue/blue shading).

the column are very different at low levels from those in the 2006 case, with the near-surface negative anomalies much weaker in this case. (compare to Fig. 5c). The relative humidity averaged over the square column is generally high from the beginning of the analysis, and θ_e increases steadily at all pressure levels as the system develops.

In summary, the genesis and early intensification of Tropical Cyclone George is different to that of the January 2006 unnamed low. The inner core atmospheric conditions in George were much more favourable for intensification, with higher values of θ_e and relative humidity throughout the troposphere (compare Fig. 10 with Fig. 5). As the moderately strong vertical wind shear decreased in magnitude, convective bursts occurred almost continuously within the column and the vortex began to intensify. However, as noted by Kilroy *et al.* (2016), it is not possible to conclude from the analyses that the decrease in vertical shear led to the intensification or whether the intensification, itself, led to the reduction in shear.

5. Formation of Tropical Cyclone Carlos (2011)

Figure 11a shows the track of Tropical Cyclone Carlos (2011) during the period of interest, while Fig. 11b shows the magnitude of the mean vertical wind shear between 850 mb and 200 mb averaged over columns 2^olat$\times 2^o$lon, 4^olat$\times 4^o$lon, and 6^olat$\times 6^o$lon centred on the location of the minimum geopotential at 850 mb. Panel (b) shows also the maximum wind speed at 850 mb within the 2^olon $\times 2^o$lat column. At the beginning of the analysis (00 UTC 13 February), the magnitude of the vertical shear is small (< 3 m s^{-1}), but over the next four days it increases in strength (with some fluctuation) reaching a maximum of about 10 m s^{-1} at 00 UTC 17 February.

The maximum 850 mb wind speed in the 2^olon $\times 2^o$lat column increases from less than 18 m s^{-1} to about 38 m s^{-1} over the first 3 days, before falling by 15 m s^{-1} over the next two days in the presence of increasing vertical wind shear. The slow moving low was named on 16 February, but was downgraded again to a tropical low on 17 February. For the next four days the system maintained its intensity despite experiencing moderate values of vertical shear. In the early hours of 21 February, the low returned to the open waters of the Indian Ocean and it re-intensified into a cyclone, the 850 mb wind speed reaching a maximum of about 45 m s^{-1} on 23 February.

Figure 12 (a,b) shows the wind structure at 850 mb together with geopotential height, while panels (c,d,e,f) show a vorticity and OW perspective of the low at 00 UTC 13 and 15 February 2011. Initially the region of strong westerlies over the northern Top End is relatively small, but over the next 48 h the westerlies increase in strength and there is a lowering of the geopotential heights near the system centre. At 00 UTC 13 February there are several regions of elevated cyclonic vertical vorticity surrounding the low centre and there are strips of vorticity to the east available to be rolled up into the low (Fig. 12c). At this time, there are only sparsely located patches of positive OW near the low centre (Fig. 12e), suggesting that immediate development is unlikely. Over the next 48 h a strong

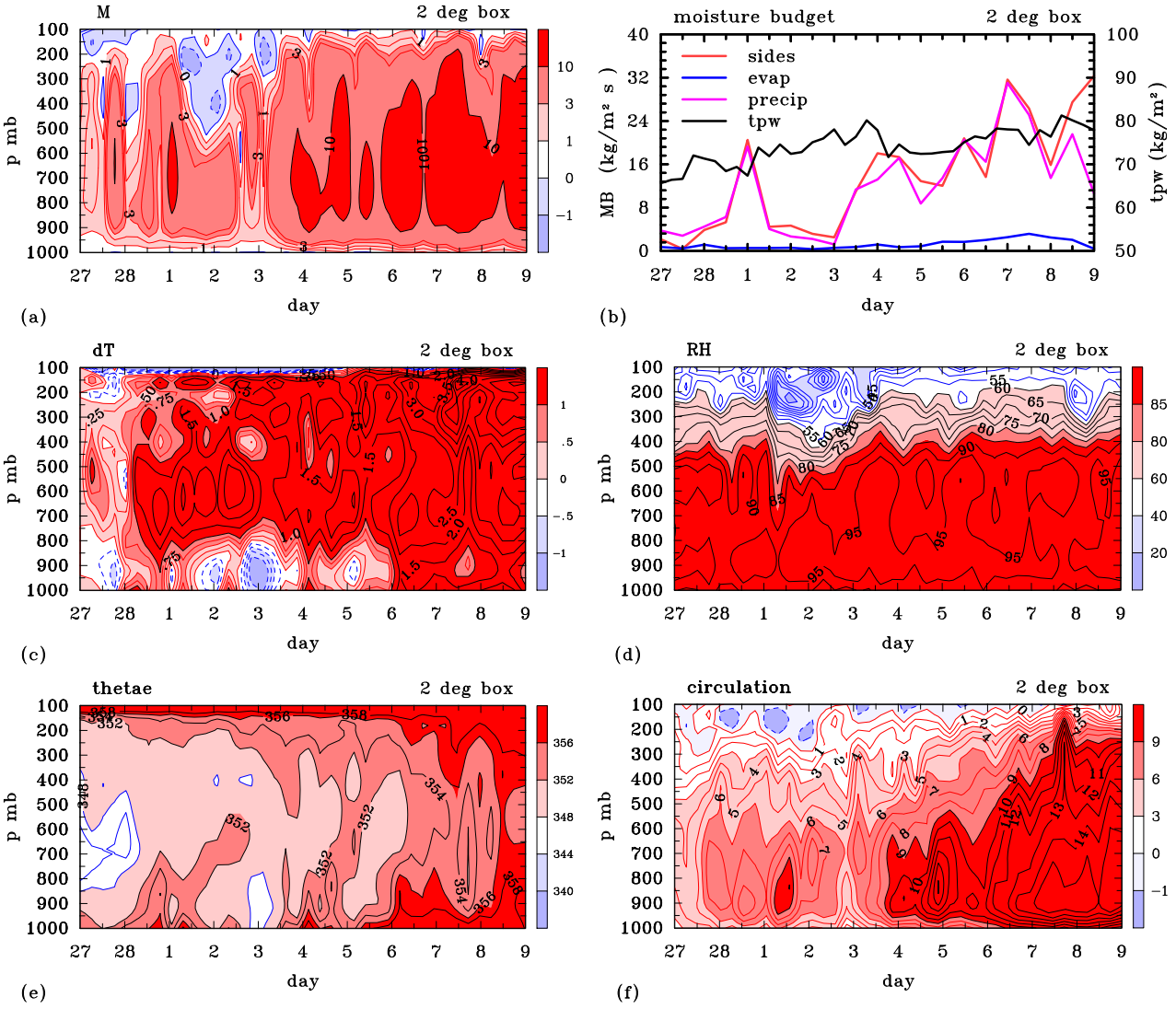

Figure 10. Time-height cross-section of system averaged quantities within a column 2^olon $\times 2^o$lat, centred on the location of the minimum geopotential at 850 mb for the development of the low that became Tropical Cyclone George. The panels have the same descriptions as those in Fig. 5.

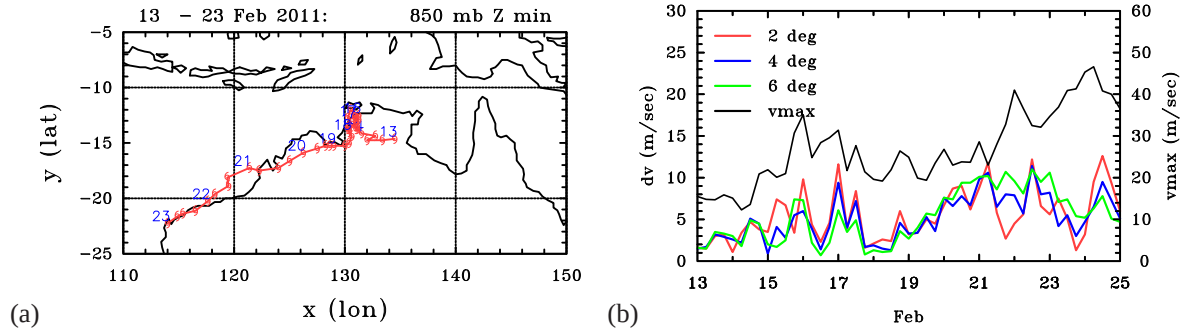

Figure 11. (a) Track of Tropical Cyclone Carlos in the Northern Territory region during the period 12 - 28 February 2011. Positions of the minimum geopotential at 850 mb indicated by cyclone symbols every 6 h. Positions at 00 UTC shown by date. (b) Mean vertical wind shear, characterized by the magnitude of the vector velocity difference between 850 mb and 200 mb, averaged over columns 2^olon $\times 2^o$lat, 4^olon $\times 4^o$lat, and 6^olon $\times 6^o$lat centred on the location of the minimum geopotential at 850 mb and maximum wind speed at 850 mb within the 2^olon $\times 2^o$lat column.

circulation develops with the region of enhanced vertical vorticity consolidating further. However, regions of positive OW remain relatively small scale compared to those in Tropical Cyclone George (compare Fig. 12f with Fig. 8).

We examine next the fields of 500 mb vertical p-velocity. These are shown in Fig. 13 at 00 UTC on 13 and 15 February 2011 with the wind vectors at 850 mb superimposed. On 13 February there are extensive regions of convection to the north and northeast of the geopotential low, but hardly any strong values (characterized by yellow contours) near the low centre at this time. On 15 February there are strong values of vertical velocity near the circulation centre (Fig. 13) reflecting the presence of strong deep convection. Such convection continues to occur near the circulation centre over the next few days (see analysis of Figure 14) in the following.

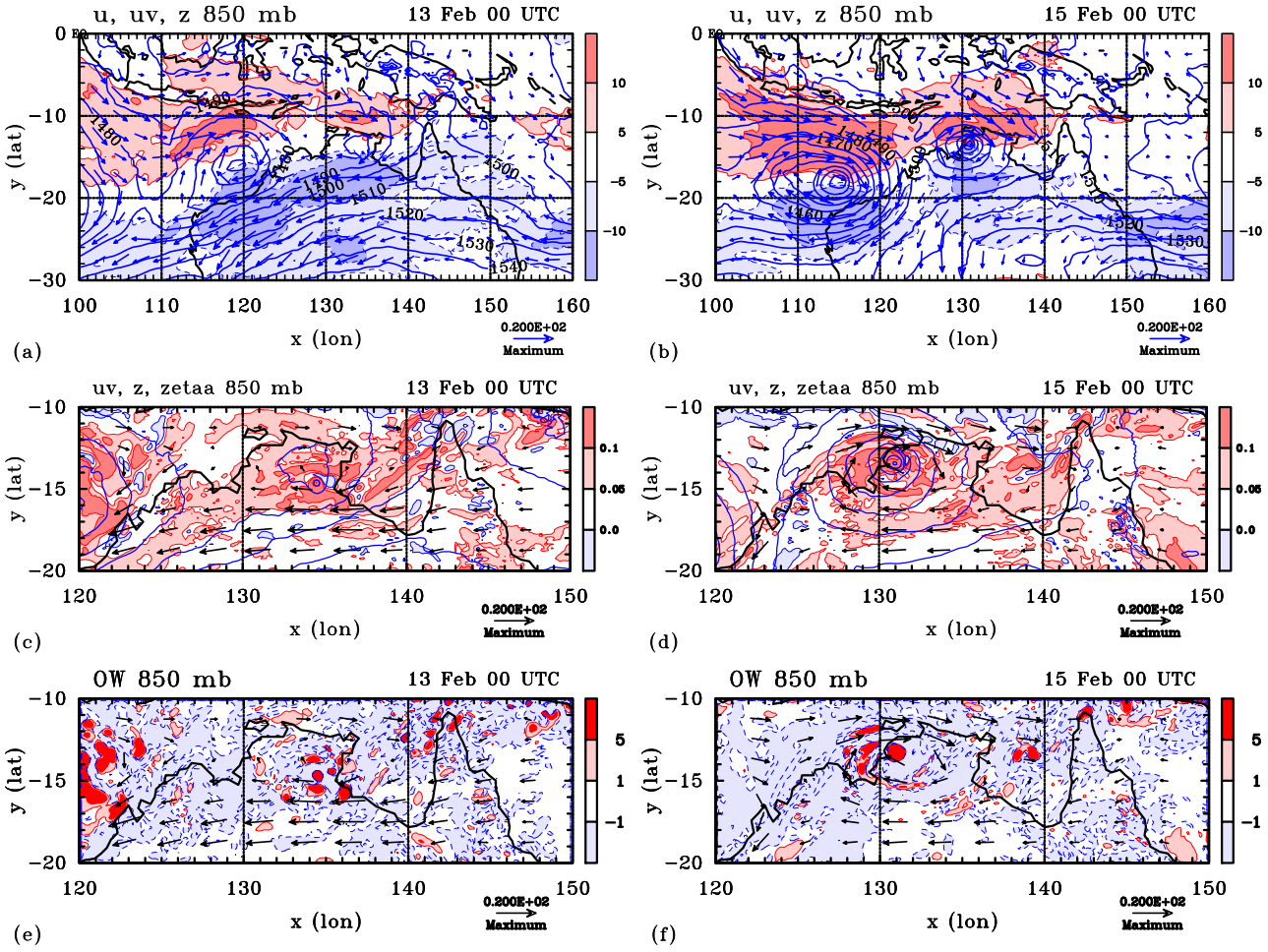

Figure 12. Wind vectors at 850 mb together with contours of the zonal wind component and geopotential height at 00 UTC on (a) 13 February and (b) 15 February 2011. Contours are the same as in Figs. 2 and 7. Wind vectors at 850 mb together with contours of the absolute vorticity (shaded) and geopotential height (thick blue contours) at 00 UTC on (c) 13 February and (d) 15 February 2011. Contours are the same as in Figs. 3 and 8 left panels. Contours of the Okubo-Weiss (OW) parameter (shaded) at 00 UTC on (e) 13 February and (f) 15 February 2011. Contours are the same as in Figs. 3 and 8 right panels. Note the different longitude scales in panels (a) and (b) compared to panels (c-f).

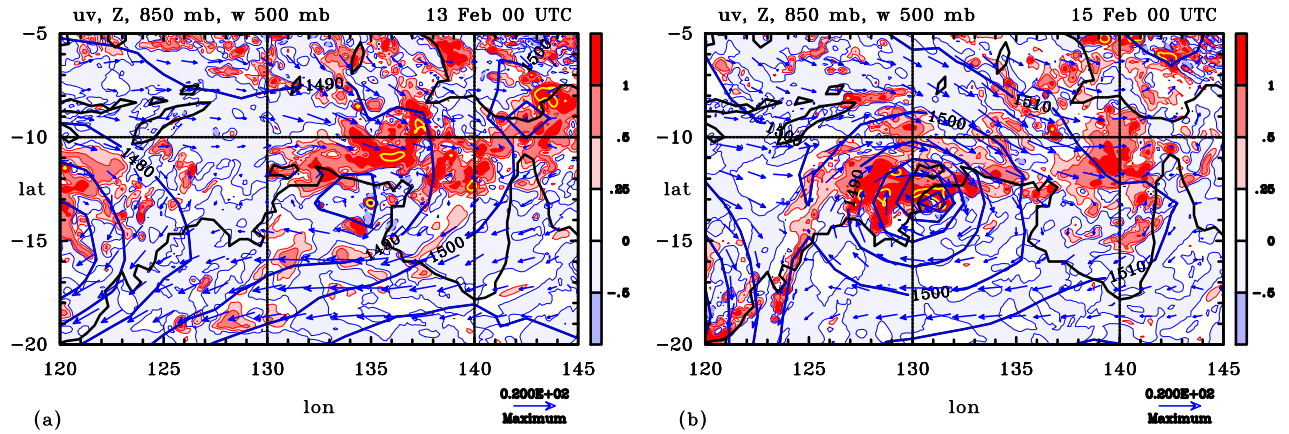

Figure 13. Wind vectors, contours of geopotential height together with contours of the vertical velocity at 500 mb at 00 UTC on 13 and 15 February 2011, illustrating the formation of tropical cyclone Carlos. Contour interval for geopotential height is 10 m. Vertical p-velocity (ω) shading as shown on the label bar in units Pa s^{-1}. Upward vertical velocities (negative values of ω) are plotted as positive (red/pink shading); negative values of vertical velocity (positive values of ω) are plotted negative (light blue/blue shading).

Figure 14 shows time-height cross sections of various quantities averaged over a mesoscale column 2^olon $\times 2^o$lat centred on the minimum geopotential at 850 mb. These quantities are the same as those shown previously in Figs. 5 and 12 for the other cases. Notable features in the vertical mass flux field are the consistently high values of positive mass flux (> 3 kg s^{-1} m^{-2}) thoughout the troposphere from 14 February onwards with a strong pulse late on 15 February leading to the local maximum in wind speed at 00 UTC 16 February (Fig. 11b). From 06 UTC 13 February onwards, the vertical mass flux is positive, the precipitation increases in strength while the transport of moisture into the

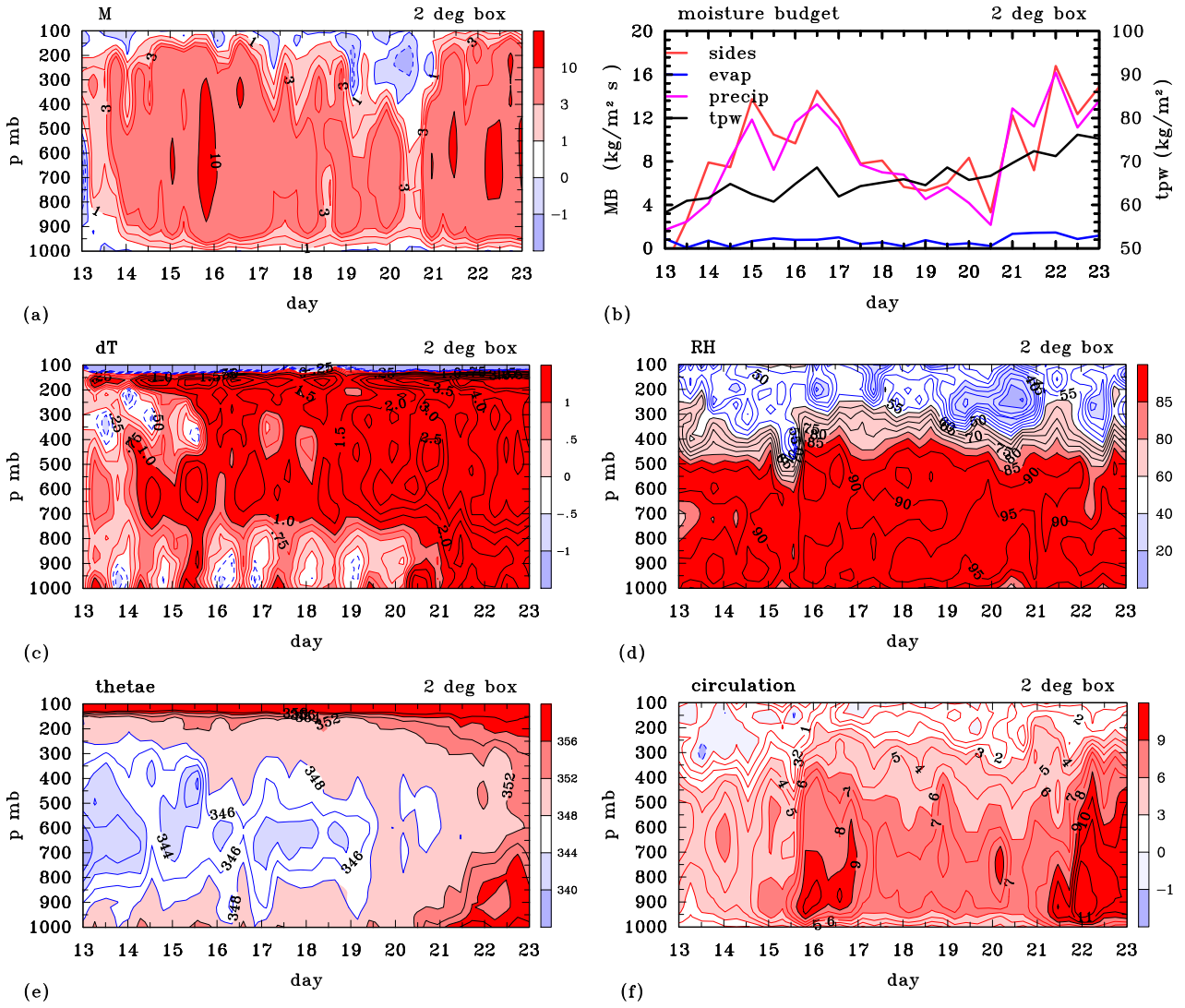

Figure 14. Time-height cross-section of system averaged quantities within a column 2^olon $\times 2^o$lat, centred on the location of the minimum geopotential at 850 mb for the development of the of the low that became Tropical Cyclone Carlos. The low was named Tropical Cyclone Carlos around 00 UTC 16 February but was downgraded to a tropical low 21 h later. The system reintensified and was reclassified a tropical cyclone at 00 UTC on 21 February. These cross-sections include (a) the vertical mass flux per unit area (units kg s^{-1} m^{-2}) (c) the temperature deviation from that at the start of the time series, (d) the relative humidity (in per cent), and (e) pseudo-equivalent potential temperature (in K). Panel (f) shows the normalized circulation around the column (units m s^{-1}). Panel (b) shows the sources and sinks of moisture including the contributions by surface evaporation, precipitation and the horizontal transport of moisture averaged over a 2^olon $\times 2^o$lat column centred on the location of the minimum geopotential at 850 mb. The horizontal transport of moisture is calculated by summing the vertically integrated fluxes of moisture into the column and then dividing the sum by the area of the column so that all terms have the units kg m $^{-2}$ s $^{-1}$. The values shown here have been multiplied by 10^5. Shown also is the total precipitable water in kg m $^{-2}$.

column is positive also. In general, the transport of moisture into the column and the precipitation are the dominant terms in the moisture budget with the moisture transport slightly exceeding the precipitation at most times. The TPW in the column shows a progressive increase over the 10 day time period shown.

Surface latent heat fluxes averaged over the 2^olon$\times 2^o$lat square column have values similar to the other lows while they were over land and over the sea. For example, the values at 00 UTC on 20 and 21 February are 106 and 302 W m^{-2}, respectively.

Temperature differences show strong mid-upper level warming throughout development, with periods of weak cooling at low levels (Figure 14(c)). As in the other cases studied, the cooling is presumably associated with precipitation from deep convection. The relative humidity in the column is generally high, mostly exceeding 85 % throughout the period shown. Throughout the troposphere, values of θ_e are the lowest of all three systems in this study and at low-levels values remain relatively low (no dark red shading) in the low-mid troposphere until 21 February. However, there are regular periods where θ_e is elevated at low levels to maintain convective instability.

The stronger bursts of deep convection (mass flux values greater than 10 kg s^{-1} m^{-2}) that occur on 15 February, and then again on 22 and 23 February are associated with increases in the circulation strength. The circulation around the 2^olon$\times 2^o$lat column begins to increase at low levels following these convective bursts. After the initial strong burst on 15 February the circulation weakens and remains moderate until 21 February, when the low moves out over the water.

In summary, the low that became Carlos experienced an environment with initially low values of equivalent

potential temperature throughout the troposphere. There was relatively weak vertical shear before 15 February, although it increased in strength between 15 - 17 February, then subsequently decreased after that. Following periods of relatively favourable vertical shear the system intensified, and it weakened in periods of unfavourable vertical shear. The circulation strength increased after a period of strong deep convective bursts near the circulation centre. Following these strong convective bursts was a period where the vertical mass flux profile was consistently positive through much of the troposphere. During this period the circulation remained relatively constant. Later, strong deep convection occurred again and the system circulation increased in strength also.

6. Discussion

The location of the monsoon shear line over the Australian continent increases the likelihood of low pressure systems forming and intensifying over land. The question arises: do such developments differ appreciably from those when the shear line is located over the sea? A comparison of the three lows examined here to the two systems analysed by Smith *et al.* (2015) that developed over the sea suggests that the answer is no. In terms of vorticity dynamics, the processes appear to be just the same. Simply, patches of low-level, convectively-enhanced vorticity in the vicinity of the monsoon shear line are converged by the broad-scale overturning circulation induced by clusters of deep convection. Above the frictional boundary layer, this convergence increases the circulation about fixed circuits encircling or within the convective region, thereby increasing the tangential wind component along that circuit. Since the absolute circulation is proportional to the absolute angular momentum, the process is equivalent (in an axi-symmetric sense) to spin up by the inward advection of surfaces of absolute angular momentum, sometimes referred to as the conventional, or classical, mechanism for spin up articulated by Ooyama (1969): see reviews by Montgomery and Smith (2014, 2016).

In both types of development, the broad-scale convectively-induced convergence brings moisture into the system which is approximately equal to the loss of moisture by precipitation. In comparison, the supply of moisture at the surface is a small fraction of the total moisture budget. Nevertheless, the surface moisture flux is essential to maintain convective instability so that deep convection in the inner core region of the low can be sustained. The maintanence of instability over land was evidenced in the analyses by regular increases in low-level θ_e.

The main difference between systems that develop over land and those that develop over the sea is the more restricted supply of surface moisture (typically 100-150 W m^{-2} maximum during the daytime compared with up to 700 W m^{-2} over the sea) and, of course, the larger friction over land. In this context, it is worth noting that, in a numerical modelling study, Montgomery *et al.* (2009) found that values on the order of 100 W m^{-2} are sufficient to support some degree of vortex intensification.

The present analyses together with those of Kilroy *et al.* (2016) and the numerical simulations of Tang *et al.* (2016) indicate that levels of total precipitable water in the monsoon environment are high, even when the monsoon shear line is over land. Thus, in the absence of appreciable vertical shear, the convectively-induced convergence will provide protection to the low from the adverse effects of dry air intrusion from the Australian continent.

In summary, echoing the previous results of Smith *et al.* (2015), Kilroy *et al.* (2016) and Tang *et al.* (2016), the results of this study suggest that the processes by which tropical lows form and intensify over land are *not* fundamentally different from those of tropical lows that form over the sea. In essence, tropical lows are warm-cored, convectively-driven vortices just like tropical cyclones.

7. Conclusions

In continuation of recent studies on the same topic, we have presented an analysis of tropical low formation and intensification over land during the Australian monsoon, based on European Centre for Medium Range Weather Forecast analyses. In particular, we examined three lows that all developed and intensified either over land or near the coast. The findings point to the generality of those in the earlier studies and identify processes that are canonical in low development.

- The analyses highlight the requirement for repeated bursts of deep convection to occur near the low centre. This convectively-induced inflow in the lower troposphere concentrates cyclonic vorticity, which increases the local circulation about the centre, thereby increasing the local tangential wind speed. Assuming approximate gradient wind balance above the boundary layer, the increase in tangential wind speed leads to a lowering of the central pressure. If deep convection diminishes (i.e. the convective mass flux declines), the low progressively weakens.
- The convectively-induced inflow in the lower troposphere imports air into the low from its moist monsoonal environment, providing an effective shield against the adverse effects of dry air intrusion from the Australian continent.
- While the contribution to the overall moisture budget by surface fluxes is relatively small, these fluxes are necessary to maintain convective instability near the vortex centre. The findings indicate that the processes of intensification are the same over land as those that operate over the ocean. Even though the surface moisture fluxes are larger when the low is located over the sea, the fluxes over land during the monsoon are large enough to support continued deep convection near the vortex centre. However, they are not large enough to allow storms to achieve more than minimal tropical cyclone, perhaps in part because of the increased surface friction over land.

Perhaps the most obvious application to forecasting is the recognition that pulses of deep convection occurring near the centre of circulation may be expected to promote pulses of intensification, whereas the absence of such convection would not.

8. Acknowledgements

GK and RKS acknowledges funding for tropical cyclone research from the German Research Council (Deutsche Forschungsgemeinschaft) under Grant no SM30/23-4 and the Office of Naval Research Global under Grant

No. N62909-15-1-N021. MTM acknowledges the support of NSF grant AGS-1313948, NOAA HFIP grant N0017315WR00048, NASA grant NNG11PK021 and the U.S. Naval Postgraduate School.

References

Bauer, P., T. Auligné, W. Bell, A Geer, V, Guidard, S Heilliette, M. Kazumori, M-J. Kim, E. H-C. Liu, A.P. McNally, B. Macpherson, K. Okamoto, R. Renshaw, L-P. Riishøjgaard. 2011: Satellite cloud and precipitation assimilation at operational NWP centres. *Q. J. R. Meteor. Soc.*, **137**: 1934-1951.

Davidson NE, Holland GH, 1987: A diagnostic analysis of two intense monsoon depressions over Australia. *Mon. Wea. Rev.*, **115**, 380-392.

DeMaria M, Kaplan J. 1994: A Statistical Hurricane Intensity Prediction Scheme (SHIPS) for the Atlantic basin. *Wea. Forecasting*, **9**, 209-220.

Dunkerton TJ Montgomery MT Wang Z. 2009 Tropical cyclogenesis in a tropical wave critical layer: easterly waves. *Atmos. Chem. Phys.*, **9**, 5587-5646.

Foster IJ, Lyons TJ. 1984: Tropical cyclogenesis: A comparative study of two depressions in the northwest of Australia. *Q. J. R. Meteor. Soc.*, **110**, 105-119.

Hendricks EA, Montgomery MT, Davis CA. 2004: On the role of "vortical" hot towers in formation of Tropical Cyclone Diana (1984). *J. Atmos. Sci.*, **61**, 1209-1232.

Kilroy G, Smith RK, Montgomery MT, Lynch B and Earl-Spurr C, 2016: A case study of a monsoon low that formed over the sea and intensified over land as seen in the ECMWF analyses. *Q. J. R. Meteor. Soc.*, **142**: in press.

May, PT, Mather JH, Vaughan G, Jakob C. 2008a: Characterizing oceanic convective cloud systems. *Bull. Amer. Meteor. Soc.*, **89**, 153-155.

May, PT, Mather JH, Vaughan G, Jakob C, McFarquhar GM, Bower KN, Mace GG. 2008b: The tropical warm pool international cloud experiment. *Bull. Amer. Meteor. Soc.*, **89**, 153-155.

McBride JL, Keenan TD. 1982: Climatology of tropical cyclone genesis in the Australian region. J.Clim., **2**, 13-33.

Montgomery MT, Nicholl ME, Cram TA, Saunders A, 2006: A "vortical" hot tower route to tropical cyclogenesis. *J. Atmos. Sci.*, **63**, 355-386.

Montgomery MT, Nguyen SV, Smith RK, and Persing J, 2009: Is WISHE essential for tropical cyclone intensification? *Q. J. R. Meteor. Soc.*, **135** 1697-1714.

Montgomery MT, Smith RK, 2014. Paradigms for tropical-cyclone intensification. *Aust. Meteor. Ocean. Journl*. (Bruce Morton Memorial Volume), **64**, 37-66.

Montgomery MT, Smith RK, 2017. Recent Developments in the fluid dynamics of tropical cyclones. *Annu. Rev. Fluid Mech.*, **49**, 1-33, doi: 10.1146/annurev-fluid-010816-060022.

Ooyama KV. 1969 Numerical simulation of the life cycle of tropical cyclones. *J. Atmos. Sci.*, **26**, 3-40.

Smith RK, Montgomery MT, Kilroy G, Tang S, Müller SK. 2015: Tropical low formation during the Australian monsoon: the events of January 2013. *Aust. Met. Ocean. Soc. Journl.*, **65**, 318-341.

Tang S, Smith RK, Montgomery MT, Gu M. 2016: Numerical study of the spin up of a tropical low over land during the Australian monsoon. *Q. J. R. Meteor. Soc.*, **142**: (in press)

Tory KJ, Montgomery MT, Davidson NE, 2006a: Prediction and diagnosis of tropical cyclone formation in an NWP system. Part I: The critical role of vortex enhancement in deep convection. *J. Atmos. Sci.*, **63**, 3077-3090.

Tory KJ, Montgomery MT, Davidson NE, Kepert JD. 2006b: Prediction and diagnosis of tropical cyclone formation in an NWP system. Part II: A detailed diagnosis of tropical cyclone Chris formation. *J. Atmos. Sci.*, **63**, 3091-3113.

Tory KJ, Davidson NE, Montgomery MT. 2007: Prediction and diagnosis of tropical cyclone formation in an NWP system. Part III: Diagnosis of developing and nondeveloping storms. *J. Atmos. Sci.*, **64**, 3195-3213.